



# Digital image analysis on cathodoluminescence microscopy images for ancient ceramic classification: methods, applications, and perspectives

E. Odelli<sup>1,2,a</sup> , F. Volpintesta<sup>3</sup>, S. Raneri<sup>4</sup> , Y. Lefrais<sup>5</sup>, D. Beconcini<sup>1</sup>, V. Palleschi<sup>4</sup> , R. Chapoulie<sup>5</sup> 

<sup>1</sup> Department of Civilization and Forms of Knowledge, University of Pisa, 56126 Pisa, Italy

<sup>2</sup> Department of Archaeology, University of Ghent, 9000 Ghent, Belgium

<sup>3</sup> School of Science and Technology, Geology Division, University of Camerino, 62032 Camerino, Italy

<sup>4</sup> Applied and Laser Spectroscopy Laboratory, Institute of Chemistry of Organometallic Compounds, Research Area of National Research Council, 56124 Pisa, Italy

<sup>5</sup> Archéosciences Bordeaux, UMR 6034, CNRS, University Bordeaux Montaigne, Domaine universitaire, 33607 Pessac, France

Received: 3 March 2022 / Accepted: 27 April 2022

© The Author(s) 2022, corrected publication 2022

**Abstract** This paper aims to investigate the application of cathodoluminescence (CL) imagery (with optical microscopy) and CL spectroscopy (with Scanning Electron Microscope) in ancient ceramics studies, for a proper classification of petro-fabrics and mineral inclusions based on their CL response. Digital image analysis (DIA) routines are proposed for both qualitative and quantitative analysis, and outcomes are reviewed in the light of classical optical microscopy (OM) and scanning electron microscopy (SEM–EDS) approaches. Obtained results demonstrated the suitability of CL in discriminating ceramic groups, offering also complementary information connected with aspects as provenance or manufacturing processes. CL imagery and spectroscopy data are also used to discuss perspectives of the method, debating bias, limits, or suspicious inconsistencies, exploring how compositional features or sample's nature imprint CL response, and finally providing the basis for future developments. Addendum at the back of the paper includes and extensively discusses some technical aspects regarding the applied DIA routines, developed in open-sources software environments and available as supplementary materials.

## 1 Introduction

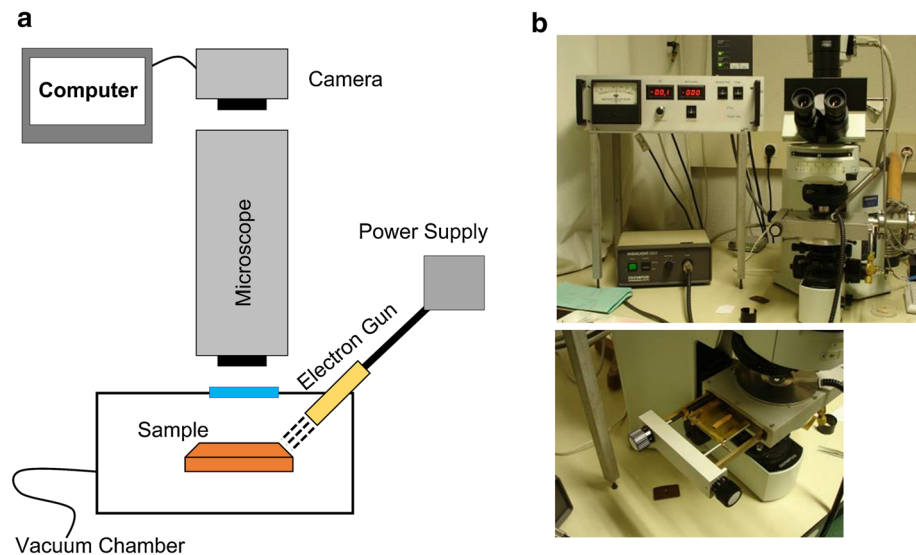
The archaeological research on material objects is nowadays more and more supported by digital image analysis (DIA) and this trend is always growing with the new possibilities offered also by open-source software [37]. Different routines and methods—from 2 to 3D digital imaging techniques—are applied on a variety of records, from small objects to whole excavated areas to keep track of their characteristics and extract qualitative and quantitative data [15, 7, 10, 14, 22, 20, 23, 2, 32].

In ancient ceramics' studies, DIA is often used to process images obtained by classical approaches like optical microscopy (OM) and scanning electron microscopy (SEM–EDS). Literature offers several examples of successful applications of DIA on polarized images [25, 3, 27] and on backscattering images and elemental maps [3, 4, 27] to implement petrographic description and grain size distribution analysis. The coupling of well-established methods based on images acquisition and DIA brought obvious advantages, especially in quantitative analysis, together with some limitations, due to the technique itself or to the difficulties in automatizing non-trivial analysis procedures [25, 27].

In the panorama of methods giving back images that can be treated with DIA, cathodoluminescence (CL) represents a promising technique for the analysis of archaeological samples [1, 13]. The method is based on the interaction between an electron beam and the sample. The electron beam interacts with objects either crystalline or non-crystalline (specifically with point defects at the atomic level in the structure) giving back a response mainly in the visible wavelength range [13, 35]. The colours of the grains can be associated with the minero-petrographic characteristics of the objects; therefore, some conclusions can be drawn on aspect as provenance or technology when applied on archaeological and geological materials [13]. Overall, among the advantages of this technique, it doesn't require complex preparation (a polished surface of a thick section is enough for the analysis, of course, thin sections can also be used), provided that the sample is small enough to fit in a void chamber, which is linked to a power supplier alimenting the electron gun. The equipment presents the advantage of being very simple and easy to run (Fig. 1). Moreover, the analysis is not time-consuming for small samples, as it is only influenced by the time required by the void chamber to obtain vacuum. Once a void is made, the electron beam is produced and strikes the sample. The CL response is collected by a camera mounted on a microscope. Once measurement parameters have been set, the image acquisition is quite fast; in the case of ceramics, to have a good quality image, the exposition time would range between 15 and 30 s, depending on the sample.

<sup>a</sup> emails: [eleonora.odelli@phd.unipi.it](mailto:eleonora.odelli@phd.unipi.it); [eleonoraodelli91@gmail.com](mailto:eleonoraodelli91@gmail.com) (corresponding author)

**Fig. 1** **a** Scheme and **b** pictures of the experimental set-up. In **b**: general view of the all system (top) and details of the chamber receiving a thin slide sample (down)



Various research can be mentioned as first attempts for studying and characterizing mineral grains by using CL, from single crystals as quartz [9, 18] and minerals which zoning is easily visible with CL imaging [19], to monomineralic materials as marbles [5, 6, 11, 13] to polymineralic systems as rocks [8]. In archaeological ceramics studies, since the first proposals, various promising results have been achieved. Picouet et al. [30] and later Huntz et al. [21] focussed their research on quartz grains—usually present as inclusions in archaeological potteries—to trace raw materials provenance. In fact, a difference in CL response can be attributed to different crystal genesis and geological environment, assuming that the firing process doesn't affect the defects in quartz crystalline structure. A more extended view on CL in archaeological potteries' studies and focussing on different mineral grains is also documented. At a descriptive level, CL has been applied in support of other techniques to characterize and classify archaeological potteries considering that similar mineralogical assemblages and chemical composition would give back similar CL signals [39, 13]. CL has been also coupled with DIA to extract important quantitative and qualitative information [1, 19], as an example, Ammari et al. [1] used CL as an independent method to check the possibility to sort ceramic samples without any other investigation methods. In respect to ceramic technology, Chapoulie et al. [12] attempted discriminating between single or double heating processes in glazed potteries looking at the intensity of the CL at the body-glaze interface. More recently, CL was used, together with optical microscopy and SEM, to better describe the firing conditions of various pottery sherds, and the thermal behaviour of mineral inclusions [16]. Finally, pottery glazes were studied by Palmara et al. [29], evidencing how different responses in CL would differentiate Hellenistic black glazes and authentic replicas.

Following these successful studies, in the present work cathodoluminescence was systematically tested on different ceramic samples (from fine-grained to coarse-grained, from thin sections to thick sections) to obtain qualitative and quantitative description of archaeological potteries, both evaluating how compositional features imprint CL response and attempting grain size distribution analysis of different mineral grains hopefully discriminated by their CL signals. Comparative analysis on polarized images (acquired by optical microscopy) and geochemical data obtained by SEM–EDS have been used to evaluate if CL can be efficiently used as independent method in the analysis of ceramic materials. The first qualitative analysis routine enables a qualitative description of ceramic assemblages, providing a quick and objective grouping of the samples based on RGB channels of CL imagery. The second quantitative description is meant to be applied on a sample selection and aims to estimate the grain size distribution of the mineral grains responding with luminescence to the electron beam, also differentiating among different mineral inclusions, exhibiting different colour. To go further in the materials characterization, CL spectra collected on mineral grains differently responding to CL are also used to show possible developments in the proposed approach.

## 2 Materials and methods

Coarse-grained and fine-grained pottery samples sectioned in thin and thick sections have been used to set the image acquisition routine (see Appendix A-online resource). For the preparation of thin sections, samples have been consolidated with epoxy resin and englobed in a polyester resin, then mounted on a glass and polished with abrasive papers and alumina powder. The analysed samples included thick sections of Late Roman amphoras (Odelli et al. 2019) and thin sections of Medieval cooking wares (unpublished); samples from the two sets of materials are composed of different mineral inclusions and grain size distribution, providing examples representative of common variability in archaeological ceramics. Preliminary petrographic analysis [33, 40] on thin sections by optical microscopy enabled classifying samples (namely cooking ware labelled as G\*) in the following petro-fabrics: micaceous

matrix with quartz, feldspars, mica, and lamproites (fabric 1), micaceous matrix and ophiolitic suite fragments with quartz and feldspars (fabric 2), spathic calcite (sometimes with the adding of organic tempers as evidenced by the elongated voids) (fabric 3) and metamorphic rock fragments (fabric 4).

Non-destructive p-XRF analysis on thick sections provided a rapid classification of amphoras according to chemical composition (Odelli et al. 2019).

On both thick sections and thin sections, images have been acquired by a cold cathode cathodoluminescence system (Cathodyne OPEA equipment updated by Microvision Instruments, Evry, France). The device is paired with a Leica M125 binocular magnifier and a Leica DFC4500 digital camera (Leica Microsystems, Wetzlar, Germany) to capture images (using LAS software). It consists of an analysis chamber surmounted by a set of spacers allowing the observation of samples of varying heights. The upper part of the chamber has a porthole and an electron gun oriented at  $40^\circ$  to the optical axis. This device makes it possible to obtain a homogeneous elliptical beam with a 13 mm long axis. Image acquisition was set in the following conditions: pressure around 50 millitorr using a micro-leak, intensity of the beam current between 100 and 200  $\mu\text{A}$ , voltage from 7.5 to 12 kV (AN: if the current is constant, the voltage undergoes slight fluctuations). Gamma parameters vary from 0.10 to 1 (with an average of 0.60) depending on the crystallinity of the matrix. Saturation and gain are constant to 1. Current, voltage and exposure time were every time checked and changed to avoid overexposure and consequently misinterpretation of the acquired images during the further digital image analysis routines. On thin section, current and voltage were set at 7.5–9 kV and 140–170  $\mu\text{A}$ , with an exposure time per capture between 22 and 31.5 s at  $2.5\times$  magnification. On thick sections, images were collected at 7.5–9 kV and 110–170  $\mu\text{A}$  with an exposure time of 19/22 s. For each sample, from 15 to 55 images were acquired and tailed together to obtain the whole section.

On a selection of samples SEM–EDS analysis coupled with single point CL has been also carried out, to correlate coloured grains with mineral identity of inclusions and go further in analysis of point defects in mineral grains. In fact, scanning electron microscopes may be equipped with a CL detector, which captures the photons emitted by a sample after bombardment with an electron beam, using a parabolic mirror that reflects photons to a light guide, and from there to a photomultiplier (PMT) tube or solid-state diode that measures the intensity of the signal. Compared to cathodoluminescence optical microscopy, SEM–CL allows much higher magnification using a scanning, focussed beam characterized by a significantly smaller spot size of about few microns. State-of-the-art instrumentation offers the possibility of analysing materials at 2 nm resolution while providing intensity and wavelength values for each point analysis or map in the 300–900 nm range; therefore, CL spectra include the near UV and near IR ranges, which may be used in the study of luminescence centres. To collect SEM–CL spectra a Gatan MonoCL3 system equipped with a retractable mirror has been used for the present investigation. The collected light was directed to the monochromator and then to a high-sensitivity PMT. The spectral range was set to 350–900 nm with acquisition time of 2 nm/sec. The grating used was a 150 lines/nm centred at 550 nm. The CL system was installed on a JEOL JSM-6460 LV. CL measurements were performed at 20 kV–20 nA; experimental conditions were set after numerous trials, as the best conditions turning in high-quality spectra. The beam at the samples is few nanometres in dimension.

Digital image analysis routines have been assessed by using ImageJ software package [34] to obtain qualitative classification of ceramics according to the dominant CL response and to describe and characterize grain size distribution.

Before classification, images have been pre-processed and normalized (see Appendix A-online resource); in fact, acquired images are affected by a non-uniform illumination due to experimental set-up (e.g. geometry of the electron gun, see Fig. 1) and suffer of variable electron beam power proper of the system. Therefore, some sample areas can respond more to CL than other ones due to illumination heterogeneity, regardless of sample nature (Fig. 2). This aspect, without the appropriate precautions, could give wrong results, especially if a threshold is needed during the images analysis. For each image a correction has been thus applied to make homogeneous illumination conditions (Fig. 3). Each image was normalized by applying a Gaussian Filter on the brightness level by choosing a Sigma (the standard deviation ( $\sigma$ ) of the Gaussian, i.e. the radius of decay to  $e^{-0.5} \approx 61\%$ ) big enough not to be influenced by the bigger and brighter particles, and small enough not to be affected by the borders contribute, turning in a good approximation of the illumination surface of the sample. Once obtained, this surface has been used to normalize the image to have a homogeneous illumination. This correction has been applied on all images acquired and, for each of them, the suitable illumination surface is automatically calculated and used to normalize the image. Another aspect requiring normalization regards the presence of small areas expected not to give any CL response. Voids of matter will obviously not produce any luminescence, likewise rich-Fe mineral phases; in fact, it is known that Fe, over a significant quantity (ca 1%) does not give back any luminescence emission [13]; however, they tend to return brightness values different from zero, credibly due to instrumental noise. As per noise, the minimum brightness value for each image has been calculated and subtracted from the whole image. It is noteworthy that this correction is specially required when comparing results obtained from multiple images, normalizing the lighting condition. As for the suitable illumination surface calculation, the image analysis calculates automatically for each image the correct value to perform the correction.

As a first step, DIA has been used on CL images to enable a fast classification based on a psychophysics approach. The method aims to reproduce the process of an operator making a colour classification based on own colour's perception, using the assumption of the Standard Observer CIE 1931 (CIE 1931; see [36, 28]), which assures a more objective analysis—not influenced by the operator, repeatability, and reproducibility together with a fast and automatic processing. The routine named CIACC (Cathodoluminescence Image Analysis Colour Classification; Fig. 4) includes both pre- and post-processing analysis, giving back a classification of images based on the prevalence of red, green or blue colour perception, which are directly related to the compositional characteristics of the

**Fig. 2** Images collected by optical microscope (transmission and reflection modes), on the bottom, and cathodoluminescence, on the top. **a** sample G375, thin section **b** sample A326, thick section **c** sample A17, thick section. Scale bar, 1 mm

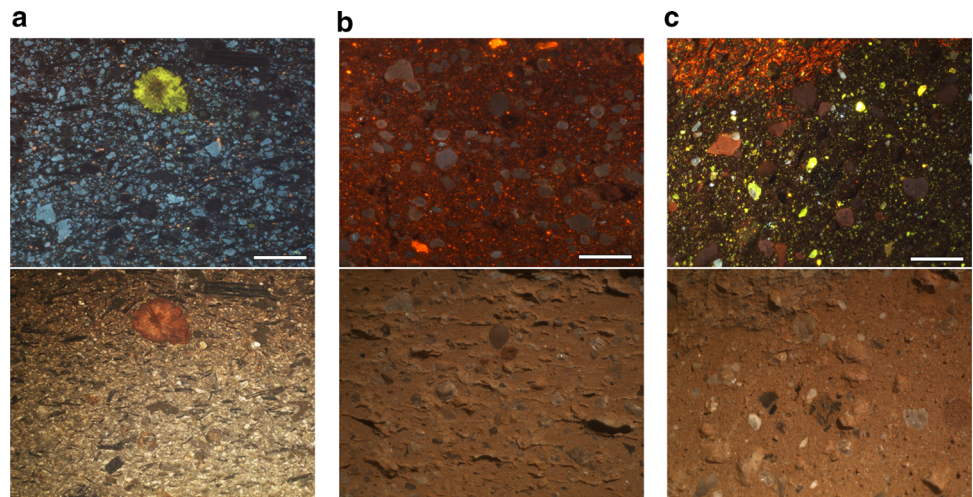


**Fig. 3** CL B/W images before **(a)** and after **b** pre-processing and normalization

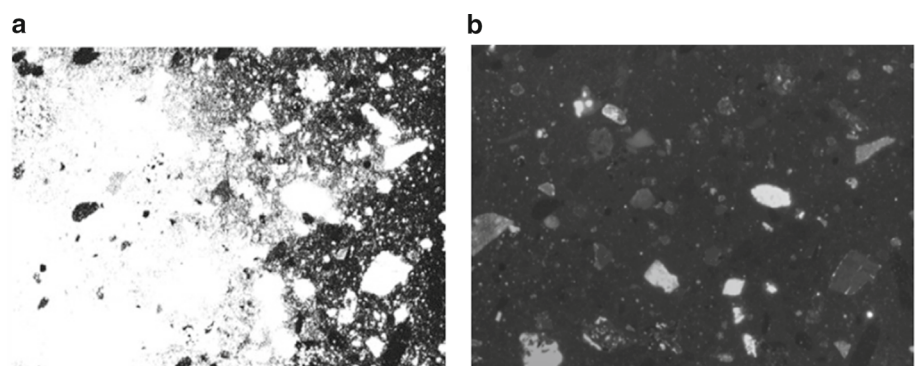
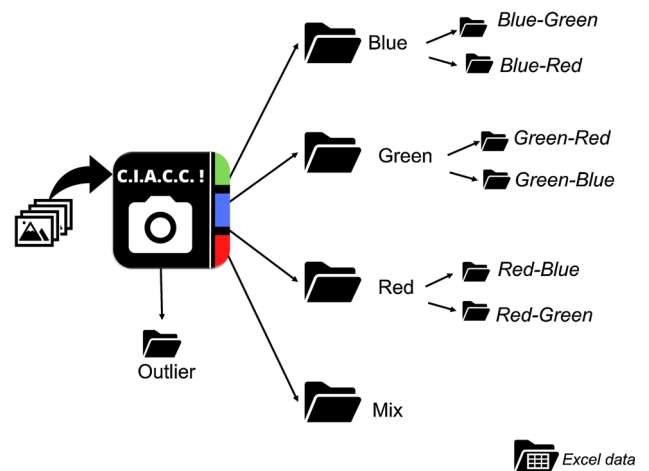


**Fig. 4** Sketch of the classification routine based on CL response and the prevalence of Red, Green, and Blue channels



analysed sample. More in detail, for all images the RGB colour components are separated, thus obtaining an image for each channel, which is multiplied by the component Y of the XYZ colour reference, to finally obtain 32-bit images representing the contribution of the chosen colour's perception for the Standard Observer. Component Y was used because it is proportional to the luminance of the colour stimulation; therefore it is the best parameter to indicate how much the selected components are perceived. Samples were thus classified basing on the dominant Red, Green or Blue response, also considering the possible prevalence of more than one channel or no channel prevailing (mix images); images too dark to give an appreciable colouring are classified as outliers.

Once samples are classified based on their CL response, a second step enabled determining quantitative parameters relevant in ceramic fabric description such as the grain size distribution of single mineralogical species; being CL sensitive to composition, different mineral phases (which identity has been checked by SEM-EDS analysis and defects inspected by CL spectroscopy) give back specific colour response in CL images so that a separation can be operated working on different channels and applied tailored image analysis routines (see Appendix B-online resource).

**Table 1** Description of the samples and classification based on CL colour perception obtained through CIACC routine

Sample ID and ceramic typology	Petro-fabric	Inclusions	CL dominant channel	Secondary CL dominant channel
G375, basin/lid	Fabric 1	Quartz, feldspars, mica, and lamproites	Blue	Green
G461-A, <i>testo</i>	Fabric 1	Quartz, feldspars, mica, and lamproites	Blue	None
G461-B, <i>testo</i>	Fabric 1	Quartz, feldspars, mica, and lamproites	Blue	None
G710-A, <i>testo</i>	Fabric 1	Quartz, feldspars, mica, and lamproites	Blue	None
G710-B, <i>testo</i>	Fabric 1	Quartz, feldspars, mica, and lamproites	Blue	None
G8, <i>olla</i>	Fabric 2	Ophiolite fragments, white mica	Green	None
G698-A, <i>olla</i>	Fabric 2	Ophiolite fragments, white mica	Green	None
G698-B, <i>olla</i>	Fabric 2	Ophiolite fragments, white mica	Green	None
G706-A, <i>testo</i>	Fabric 2	Ophiolite fragments, white mica	Green	None
G706-B, <i>testo</i>	Fabric 2	Ophiolite fragments, white mica	Green	None
G358, <i>olla</i>	Fabric 3 (a)	Sparry calcite, quartz, feldspars	Mix	None
G406, <i>olla</i>	Fabric 3 (a)	Sparry calcite, quartz, feldspars	Red	None
G412, <i>olla</i>	Fabric 3 (a)	Sparry calcite, quartz, feldspars	Mix	None
688, <i>olla</i>	Fabric 3 (a)	Sparry calcite, quartz, feldspars	Red	None
G576, <i>olla</i>	Fabric 3 (b)	Sparry calcite	Green	None
618, <i>olla</i>	Fabric 3 (b)	Sparry calcite	Red	None
G697-A, <i>olla</i>	Fabric 3 (b)	Sparry calcite	Red	None
G697-B, <i>olla</i>	Fabric 3 (b)	Sparry calcite	Red	None
G402-A, <i>olla</i>	Fabric 4	Metamorphic rock fragments	Red	Green
G402-B, <i>olla</i>	Fabric 4	Metamorphic rock fragments	Green	Red
G662, <i>olla</i>	Fabric 4	Metamorphic rock fragments	Green	None

### 3 Results and discussion

#### 3.1 CL classification and petro-fabrics

A first check of CIACC's reliability was made with a simple internal check. For some of the selected samples, two frames taken from the same section were processed and classified according to the established routine; in case of homogeneous samples (in texture and structure), frames are correctly classified within the same colour-dominant group, proving the affordability of the routine. However, it is always recommended to collect and process images describing the entire sample section and representativeness of the possible variability of the ceramic fabric to avoid misinterpretation. The CIACC routine was thus applied on the overall CL images acquired on the ceramic samples, and it took some seconds for the automatic processing of each image. The normalized images were then automatically classified based on the prevalence of RGB channels, namely red, blue or green, even considering possible outliers (i.e. when the image is too dark to offer a clear outcome) or mixed outcomes (none of the chromatic components prevailing). Further sub-division identifies a possible second dominant colour perception, evidencing variability within the same group.

The routine was applied on images acquired on both thin sections and thick sections enabling to classify studied objects and get some consideration regarding CIACC routine outcomes on different sample typologies. DIA and data extracted from images (see Appendix A) would suggest that working on a thin section better enhances the contribution of mineral grains, while working on thick sections more information on the matrix can be obtained. In both cases, low voltage and high exposure time (avoiding saturation

**Fig. 5** Examples of CL images collected on thin sections and coarse-grained potteries revealing a dominant RGB channel imprinted by compositional features. **a** G406, fabric 3-a; **b** 710-A, fabric 1; **c** G8-A, fabric 2; **d** G412, fabric 3-a; **e** G402-B, fabric 4; **f** G375 fabric 1. Scale bar = 1 mm

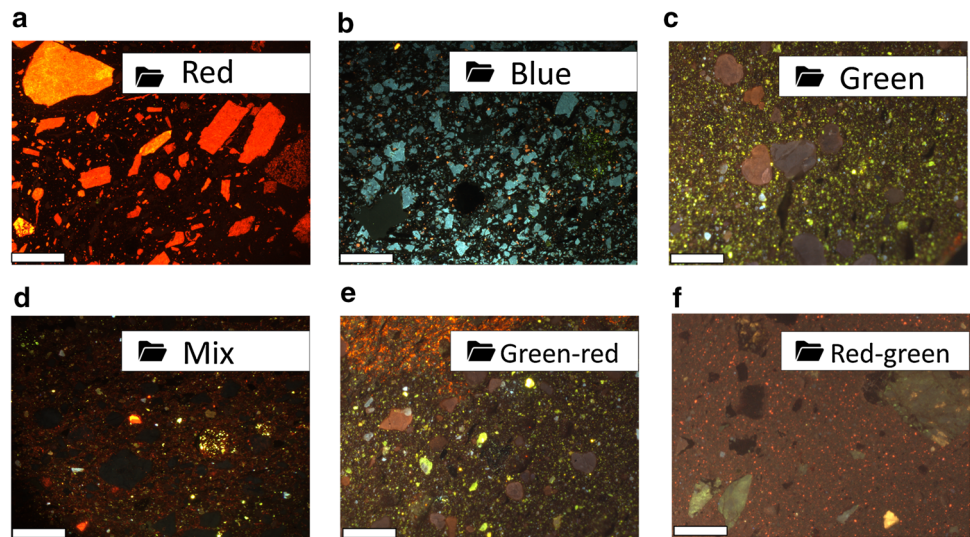
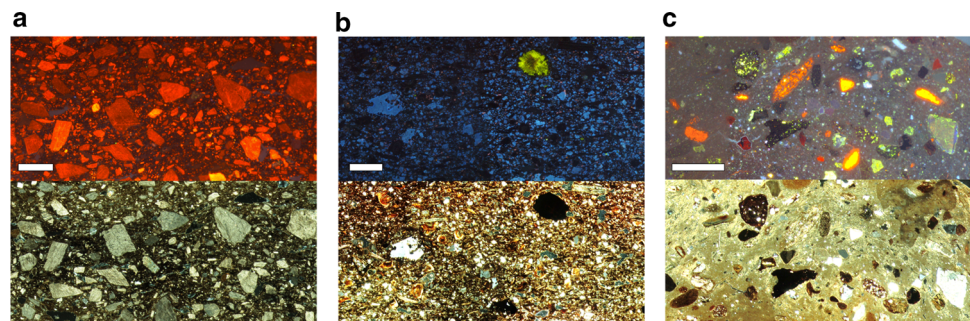


**Fig. 6** Comparison between cathodoluminescence (top) and crossed-polars images (down). **a** Fabric 3, calcite inclusions; **b** Fabric 1, feldspars, mica, and quartz inclusions; **c** Fabric 4, metamorphic rock fragments inclusions



effects) are recommended to obtain images efficiently revealing the different components of the ceramics paste (i.e. matrix, mineral grains).

For further considerations, we henceforward consider the case of image acquisition on thin sections with the aim of comparing outcomes CL and petrography. Overall, the results show good agreement between CL and minero-petrographic classification (Table 1, Fig. 5).

Samples belonging to Fabric 1, containing quartz, feldspars, mica and lamproite fragments exhibit a blue colour prevalence in CL images, except for the only “*lid/basin*” in the group (sample G375), which is classified as blue-green; in fact, as evidenced by optical microscopy, mineral components exhibiting a green CL signal are frequent, credibly related to secondary phases. This component does not influence the general fabric classification, imprinting the secondary dominant CL channel during the image analysis. Samples belonging to Fabric 2, characterized by ophiolite fragments, exhibit a dominant CL green colour. Otherwise, calcite-rich fragments belonging to petrofabric 3 are red/orange dominant due to the intense CL signal from sparry calcite grains [11] (Fig. 6). Contrary to the expectation, only one sample within the sparry calcite petro-fabric is classified as green-dominant (*sample G576*). Minero-petrographic analysis might justify this apparent inconsistency; in fact, petrographic observation reveals that calcite grains are still recognizable by their morphology, but textural features are clearly obliterated due to firing (Fig. 7). In calcite, the CL signal is related to Mn luminescent centres; thus, the obtained results would correlate with the different CL emission in a change of Mn at atomic level. This example is of high relevance for this study, suggesting that beside mineralogical features, also firing processes could greatly imprint the CL response. Finally, for samples classified in Fabric 4 (metamorphic rock fragments), the rich variety of mineral grains in rock fragments do not provide any CL dominant colour, beside green and red are the main perceived channels; as an example, we can consider two frames (A and B) from the same sample belonging to the metamorphic group (*sample G402*). Picture A is classified as red–green while picture B is recorded as green–red; even if the two main colours are registered by our CIACC routine, the textural heterogeneity and the nature of mineral grains prevents a univocal classification (Fig. 8).

It is noteworthy that, contrary to minero-petrographic classification, which considers microstructure among descriptive parameters defying petro-fabrics, CL methods and CIACC classification exclude the non-luminescent part of the image (e.g. voids or Fe-rich phases); therefore, nothing about the microstructure can be said by this technique. As an example, in red-dominant group all samples bearing sparry calcite are clustered together, regardless of microstructure features; nevertheless, petrographic observation evidenced—within this group—the occurrence of samples discriminated by the presence of elongated voids due to the addition of organics (Fig. 9). Similarly, iron-rich fragments are black in CL images and do not contribute to the colour classification (Fig. 10).

**Fig. 7** **a** CL and **b** crossed-polar images for sample G576. In figure **(b)** calcite grains optical properties are visibly altered, turning in absence of red luminescence in **(a)**. Scale bar = 1 mm. Circle and triangles are used to mark crystals localization in the different imagery acquisition

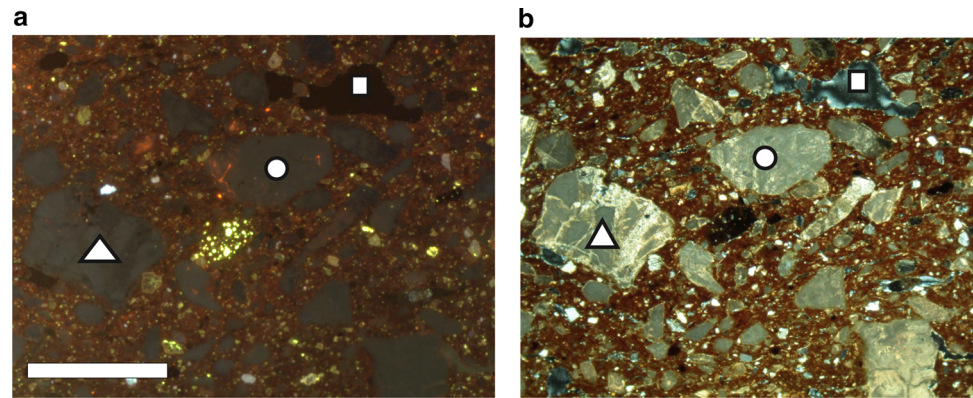
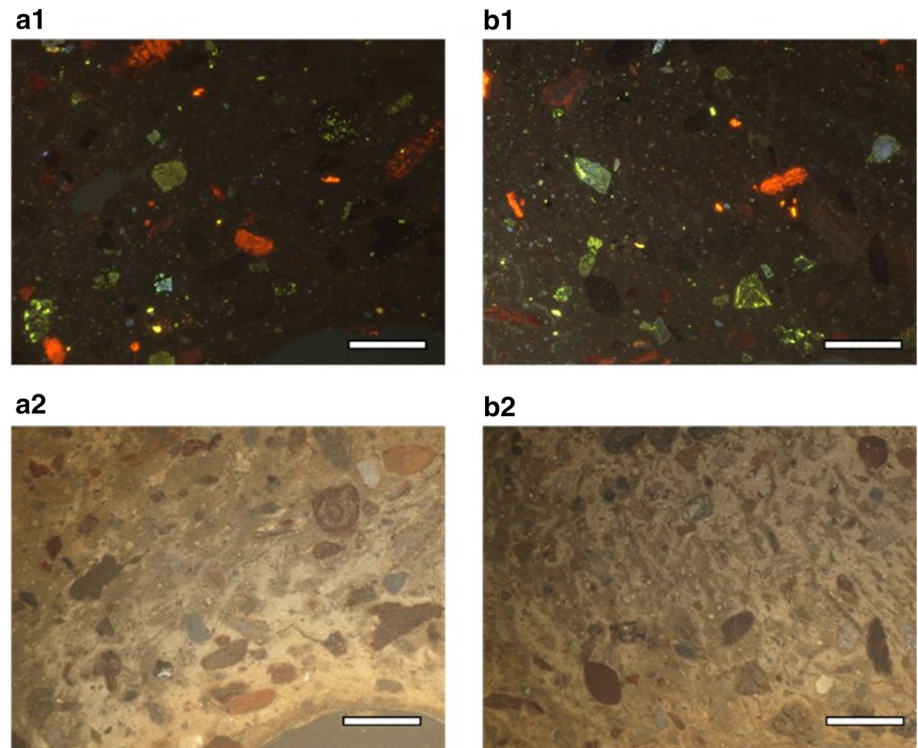


**Fig. 8** Comparison of the two images chosen to represent sample G402, fabric 4 (metamorphic rock fragments). **a** G402-A, classified as Red–green **b** G402-B, classified as Green–red. **a.1** and **b.1** images taken in cathodoluminescence; **a.2** and **b.2** images taken in normal reflected light. Scale bar = 1 mm



### 3.2 Analysis of mineral inclusions: grain size distribution and crystal defects

DIA applied on CL images (Fig. 11) demonstrated its suitability in quantitatively esteeming the grain size distribution of CL active mineral grains, differentiating their occurrence and phase abundance (%) based on CL response (Table 2; Fig. 11) (see macro developed under Image J, Appendix B). Results can provide additional information on ceramic fabric, namely textural features of specific inclusions, which respond in different way to CL, enabling to implement fabric description and highlight possible variability in the same fabric and CL group, which can be in turn correlated to different manufacture choices. As already discussed before, one of the drawbacks of this routine is that it is impossible to quantify inclusions not responding to CL, as we can notice in samples G461 and G710; the iron-rich inclusions result black in the images, and they are not counted in the area percentage. Therefore, this technique offers a good esteem for samples with a good response to CL, containing low or no iron-rich aplastic inclusion. Anyway, when iron-rich inclusions are present, the blindness of the technique must be taken into account.

Therefore, to integrate quantification of grains with compositional issues, cathodoluminescence needs a support technique to establish the correspondence of colours and mineral phases; once the correspondence is defined—even using a small selection of samples—objects can be analysed in large amount based on CL signals. In this study, SEM–EDS has been used to analyse CL-coloured grains and inform us about their mineral identity, thus enabling to provide classification of grains based on mineralogy. For example, blue grains are rich in silica, alumina and potassium, indicating feldspars; red grains are primarily composed of calcium confirming their mineral identity as calcite according to the red–orange luminescence; finally, green–yellow grains respond to plagioclase composition (see Table 3). Thus, based on this correspondence, it is also possible to quantify the distribution of those

**Fig. 9** CL vs microstructure. The two samples **a** G406 and **b** G618 are characterized by calcite mineral grains as tempers, marked by their intense red–orange CL signal and different microstructure; sample G406 **a2** optical microscope image exhibits elongated voids (dotted line) not present in sample G618 **b2** optical microscope image). CIACC routine based on CL colour perception cannot recognize differences in microstructures, as voids do not respond to CL. Scale bar = 1 mm. Circle and triangles are used to mark crystals localization in the different imagery acquisition

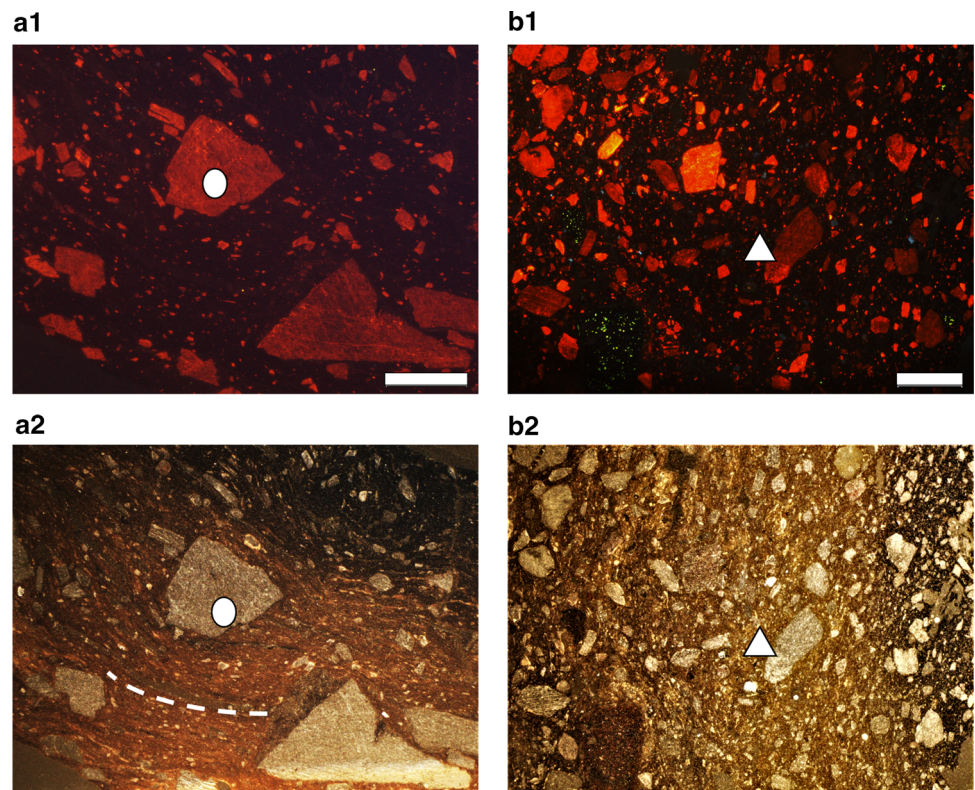
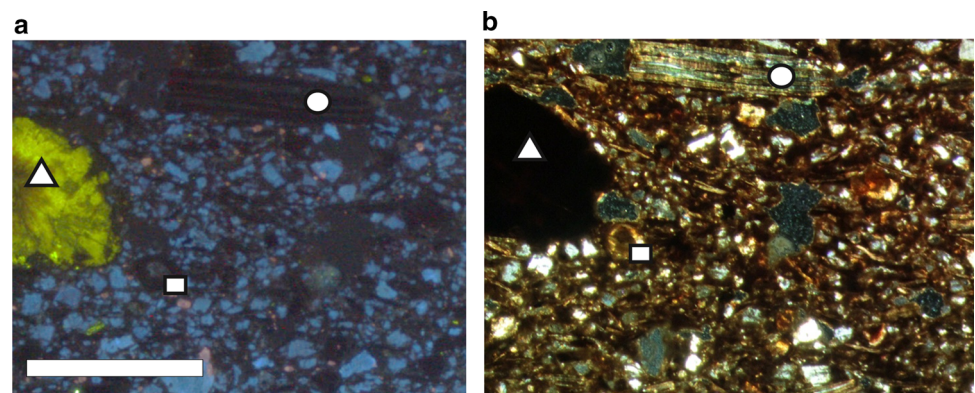


**Fig. 10** Focus on iron-rich mineral phase, exhibiting no CL, thus appearing black in the picture. **a** CL image; **b** image taken at the petrographic microscope, XP. Scale bar = 1 mm. Circle and triangles are used to mark crystals localization in the different imagery acquisition



mineral grains and compare their abundance among samples belonging to the same compositional groups, which can be relevant in improving fabric description and, in some case, support precise questions regarding technological issues.

For further developments, CL spectra collected on mineral grains might lead to the identification of luminescent centres which result from the presence of point defects (either structural defects or chemical impurities) resulting from different events that may have occurred during the lifetime of the mineral [13, 16, 38]. Here, the blue-appearing CL grains (Fig. 12a) exhibit several bands, picking at 390, 430, 460, 690, and 740 nm; the more intense bands in the blue range (390, 430 and 460 nm) can be interpreted as due to internal defects: 390 nm emission band is correlated to  $\text{SiO}_4$  tetrahedra, when an electron is moved from O to Si; the luminescent centre is described as  $\text{SiO}_4^{4-}$  ([24], MC Keever SWS, 1984). For the 430–460 nm emission band, they are possibly due to a hole centre existing between O- and  $\text{Al}^{3+}$ ; this is the strongest emitting centres in the Na–K feldspars. For the smaller red bands (690 and 740 nm), they are interpreted as due to impurities in very low concentrations like iron [26]. As for the green–yellow grains (Fig. 12b) and the red grains (Fig. 12c) the dominating emitting bands that confer the perceived colour to the grain in CL imagery, are due to the manganese impurity. For the green–yellow it is  $\text{Mn}^{2+}$  while replacing  $\text{Ca}^{2+}$  in a specific atomic environment of a plagioclase mineral, that is regarded as responsible for the CL emission [17]. While for the red grain, it is again  $\text{Mn}^{2+}$  in replacement of  $\text{Ca}^{2+}$ ,



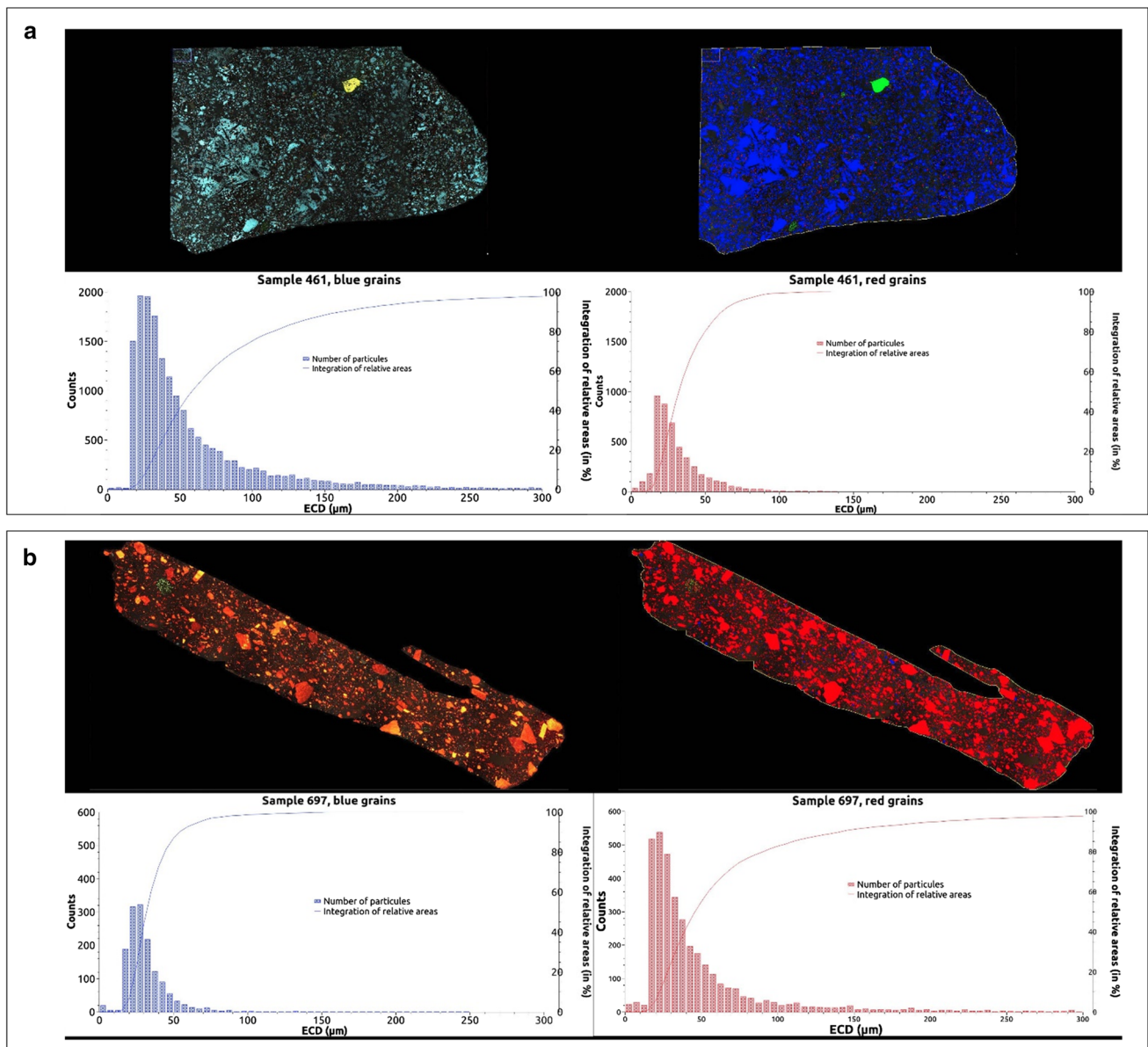


**Fig. 11** Images of the two samples during DIA and grain size distribution in ECD (Equivalent Circle Diameter in  $\mu\text{m}$ ) for **a** samples 461 (data treatment, ICA) and **b** 697 (data treatment, PCA). Counts, on the Y-axis represent the number of grains counted

but in another type of environment (i.e. a calcite crystal) that is responsible for it. In the case of the green grain (Fig. 12b), it is noticeable that a near UV band shows up at around 380 nm; it is also attributed to the silicate centre  $\text{SiO}_4^{4-}$ . The 750 nm band can be attributed to the presence of very low amounts of  $\text{Fe}^{3+}$ , but in this case the dominating band is in the green at 550 nm which gives the global green perception by the eye. For the red grain (Fig. 12c) another small and large band is seen, which maximum is in the near UV range (380 nm); this might be due to internal defects linked with oxygen vacancies in the carbonate network.

**Table 2** Grain size analysis results obtained by applying the developed DIA routine (see Appendix B-online resource)

Sample/Fabric	Method used	Grains' colour	Area (%)
461, fabric 1	<b>ICA</b>	Red	1.0
		Green	0.5
		<b>Blue</b>	<b>28.4</b>
710, fabric 1	<b>ICA</b>	Red	0.8
		Green	0.4
		<b>Blue</b>	<b>28.9</b>
698, fabric 2	<b>ICA</b>	Red	0.9
		<b>Green</b>	<b>6.6</b>
		Blue	4.1
706, fabric 2	<b>ICA</b>	Red	1.4
		<b>Green</b>	<b>10.3</b>
		Blue	0.5
406, fabric 3.a	<b>PCA</b>	<b>Red</b>	<b>23.2</b>
		Green	0.5
		Blue	0.0
697, fabric 3.b	<b>PCA</b>	<b>Red</b>	<b>28.2</b>
		Green	0.3
		Blue	1.1
662, fabric 4	<b>ICA</b>	Red	1.6
		<b>Green</b>	<b>3.4</b>
		Blue	0.1

The routine used is clarified in bold. The bold italic underlines the prevailing colour among the RGB channels

**Table 3** Chemical composition of mineral grains responding blue, green and red to CL microscopy obtained by SEM–EDS point analysis on two samples classified as red-dominant (G697) and blue-dominant (G461), as examples

Sample ID	Grains' CL colour	Elements										
		%Na	%Mg	%Al	%Si	%P	%K	%Ca	%Ti	%Mn	%Fe	%Ba
G461	Blue grain 1	2.5	0.3	<b>18.8</b>	<b>64.1</b>	0.2	<b>11.9</b>	0.4	0.3	–	0.6	0.5
	Blue grain 2	2.5	0.5	<b>18.8</b>	<b>64</b>	0.2	<b>11.6</b>	0.7	0.3	–	0.7	0.3
	Blue grain 3	2.2	0.5	<b>18.8</b>	<b>64.3</b>	0.2	<b>12.2</b>	0.6	0.2	–	0.7	0.1
	Green grain 1	0.7	1.7	<b>14.1</b>	<b>42.2</b>	0.9	5.5	1.9	0.8	0.5	<b>31.2</b>	–
	Red grain 1	0.4	0.9	2.7	<b>9.3</b>	<b>36.2</b>	1.1	<b>47.8</b>	0.1	–	1.1	–
	Red grain 2	0.4	1.2	2.7	<b>6.9</b>	<b>37.5</b>	0.6	<b>48.6</b>	0.2	–	1.2	–
	Red–orange grain 1	0.2	1.2	2.4	<b>7.7</b>	<b>37.3</b>	0.6	<b>48.5</b>	0.2	–	1.5	–
Yellow grain 1	<b>6.4</b>	3.8	<b>18.3</b>	<b>54.1</b>	1.1	0.8	2.4	1.6	2.3	<b>8.7</b>	0.2	
G697	Blue grain 1	2.4	0.1	<b>18.8</b>	<b>63.2</b>	0.1	<b>10.8</b>	0.2	0.2	1.8	1.1	0.1
	Blue grain 2	1.8	0.1	<b>19.3</b>	<b>63.1</b>	0.1	<b>11.4</b>	1.1	0.2	1.1	1	0.2
	Blue grain 3	2.3	0.1	<b>19.3</b>	<b>63.9</b>	–	<b>11.2</b>	2.1	0.2	–	0.7	–
	Blue grain 4	1.9	0.1	<b>19.4</b>	<b>64.1</b>	0.1	<b>11.4</b>	1.4	0.2	–	0.7	0.2
	Green grain 1	<b>9.2</b>	0.2	<b>19.1</b>	<b>66.1</b>	0.1	0.5	0.9	0.1	1.7	1.8	–
	Red–orange grain 1	0.6	0.5	1.4	7.4	–	0.3	<b>87.1</b>	0.2	–	1.3	–
	Red–orange grain 2	0.3	0.5	3.2	11.3	–	0.3	<b>81.9</b>	0.3	0.2	1.4	–
Red–orange grain 3	0.6	0.6	1.5	7.4	–	0.2	<b>86.9</b>	0.2	–	1.6	–	

The major elemental percentages are in bold, to better discriminate the possible diagnostic minerals present

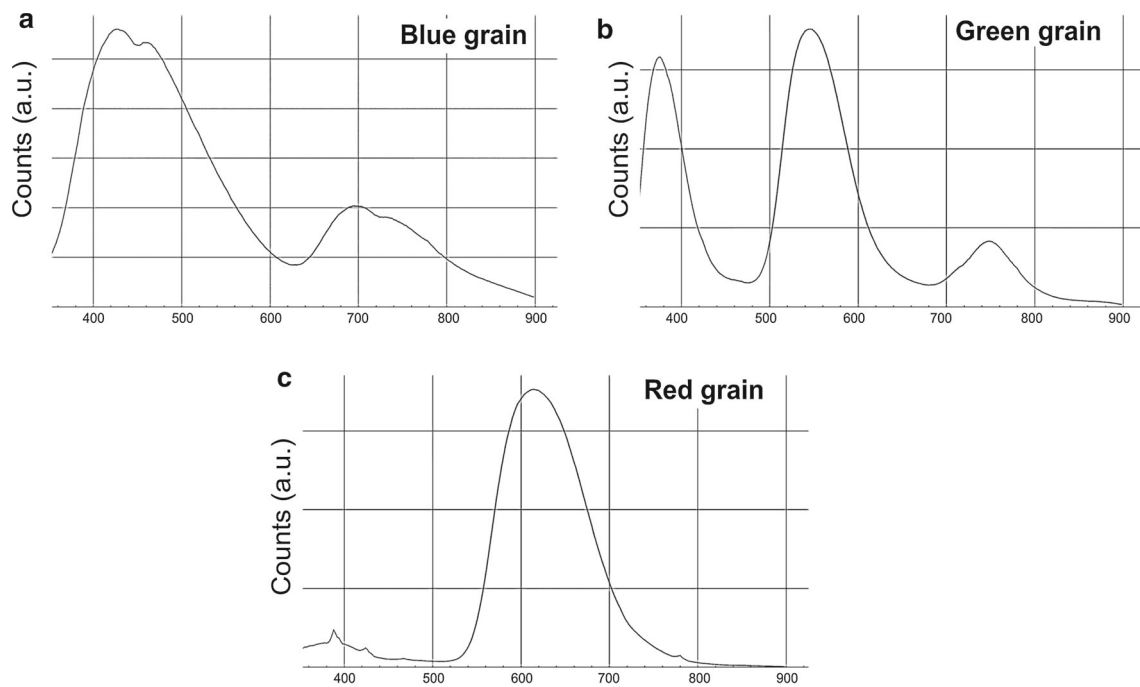


**Fig. 12** Representative CL spectrum of **a** blue grains (in CL imagery, feldspars) from sample G461; **b** green–yellow grains from sample G967 (in CL imagery, plagioclase), and **c** red grains (in CL imagery, calcite) from sample G697, as examples

#### 4 Conclusions

Cathodoluminescence coupled with DIA demonstrated to be a useful tool both in qualitative and quantitative approaches in archaeological ceramics' studies. The qualitative classification of ceramic assemblages obtained with CIACC routine and based on colour perception by CIE standard observer enables discriminating potteries according to petrofabric classification, providing also relevant information on mineralogical composition based on CL response of mineral grains. In fact, the overall CL signal is consistent with composition.

The selection of areas of interest on which collect CL images is critical for the correct classification of samples; in fact, it is advisable to tie different frames covering the entire sample surface avoiding misclassification due to a possible heterogeneity in sample texture and mineral grains' thickening and sorting. The method is reliable on thin and thick sections, providing a polished surface required for the analysis; however, statistical comparison would promote analysing thin sections when quantitative data on mineral grains have to be extracted.

Another issue is related to firing temperature which might alter the crystal features of mineral grains and thus the CL response; overfired fragments might be misclassified or poorly studied on their CL images. Moreover, the classical petrographic analysis greatly considers the contribution of microstructure, imprinted by construction method, moulding and technical issues; otherwise, voids are not sensitive to CL preventing the analysis of microstructural features on image acquisitions. Similarly, iron-rich phases, again of great interest in petrographic analysis do not respond to CL excitation, not contributing to the analysis of mineral grains.

Quantitative information on grains has been also extracted by dedicated routine, providing data on textural features of inclusion useful for comparative analysis. Moreover, the support of SEM–EDS analysis on single grains responding differently to CL demonstrated the suitability of the method in determining grains size distribution, size and shape parameters of coloured grains discriminating the contribution of different mineral inclusions, when correspondence between CL luminescence—composition of mineral grains has been addressed by microchemical analysis. This approach cannot be conclusive when looking at the distribution of the overall mineral phases but can be beneficial in archaeological studies when the presence of specific mineral phase can be relevant for provenance or technological issue. Similar conclusion could be addressed by processing SEM–EDS maps; however, CL seems to be faster enabling to focus on larger area and providing data on a lot of grains in few seconds of acquisition, differently from SEM–EDS for which small areas can be acquired and focussed on a single—usually time-consuming—acquisition. Further comparative studies would enable to highlight quantitative differences on grain size analysis obtained from images acquired by the two methods, especially for including in the analysis the whole mineral grains which overall grain-size evaluation is relevant in fabric description.

Possible further development by analysing CL spectra has been also presented; CL bands could be revealed using dedicated software for deconvoluting the spectra for a more precise analysis. This aspect is of relevance when provenance studies are part of

the investigation program, and the identification of all defects in mineral grains is seen as another way of bringing more information on geological environment of raw materials.

In the present study, CL imaging and spectroscopy were only focussed on objects classification and grain size analysis; however, this systematic study builds the basis for future developments to enlarge applications. In this perspective, analysis of mock-ups made by using different clays and fired at different temperature ranges might help in evaluating how firing temperature imprints CL signal regardless of composition [31]. Studies of defects on minerals grains from bearing ceramics from different geological environments might reveal easy, fast and reliable method in discriminating provenance. Finally, regarding quantification, systematic comparative analysis with other acquisition methods (such as petrography and SEM–EDS) is of interest for properly comparing images acquired by various methods and correctly interpret data also considering limits of the technique itself or difficulties in automatizing non-trivial analysis procedures. These are relevant issues for future successful research unveiling how CL imagery with optical microscopy and CL spectroscopy can serve ancient materials studies.

**Supplementary Information** The online version contains supplementary material available at <https://doi.org/10.1140/epjp/s13360-022-02774-9>.

**Acknowledgements** E. O. acknowledges the Tuscany Region for her PhD fellowship under the project Giovani Si, Pegaso. Some of the work carried out with CL equipment at Bordeaux, was supported by the University Bordeaux Montaigne, the CNRS and the French National Research Agency within the framework of the cluster of excellence Laboratoire des Sciences Archéologiques de Bordeaux (ANR-10-LABX-52).

**Authors' contributions** EO was involved in data handling and realization of figures. EO and DB were involved in data collection. EO, SR, RC, FV and YL were involved in draft writing. FV was involved in realization of CIACC macro and data analysis. SR and RC were involved in ideation. SR, EO and RC were involved in data interpretation. SR, VP and RC were involved in methodology and supervision. FV and YL were involved in appendix writing. YL was involved in realization of macro for quantitative analysis. RC was involved in funding. All writers reviewed, corrected, and approved the final draft.

**Funding** Open access funding provided by Università di Pisa within the CRUI-CARE Agreement. Eleonora Odelli PhD fellowship is funded by Tuscany Region thanks to project GiovaniSi. Diletta Beconcini received the Erasmus plus mobility for her stay in Bordeaux. Some of the work carried out with CL equipment at Bordeaux, was supported by the University Bordeaux Montaigne, the CNRS and the French National Research Agency within the framework of the cluster of excellence Laboratoire des Sciences Archéologiques de Bordeaux (ANR-10-LABX-52).

**Data availability** This manuscript has associated data in a data repository. [Authors' comment: The datasets generated and analysed during the current study are available from the corresponding author on reasonable request.]

## Declarations

**Conflict of interest** The authors have no competing interests to declare that are relevant to the content of this article.

**Open Access** This article is licensed under a Creative Commons Attribution 4.0 International License, which permits use, sharing, adaptation, distribution and reproduction in any medium or format, as long as you give appropriate credit to the original author(s) and the source, provide a link to the Creative Commons licence, and indicate if changes were made. The images or other third party material in this article are included in the article's Creative Commons licence, unless indicated otherwise in a credit line to the material. If material is not included in the article's Creative Commons licence and your intended use is not permitted by statutory regulation or exceeds the permitted use, you will need to obtain permission directly from the copyright holder. To view a copy of this licence, visit <http://creativecommons.org/licenses/by/4.0/>.

## References

1. F. Ammari, N. Del-Solar-Velarde, R. Chapoulie, B. Bousquet, Chemometrics applied to cathodoluminescence images: a new approach to classify pre-Columbian artefacts from northern Peru. *Environ. Sci. Pollut. Res.* **24**(3), 2205–2209 (2017). <https://doi.org/10.1007/s11356-016-7992-3>
2. F. Anichini, F. Banterle, J. Garrigós, M. Callieri, N. Dershowitz, N. Dubbini, D.L. Diaz, T. Evans, G. Gattiglia, M.L. Gualandi, M.A. Hervas, B. Itnik, M. Madrid i Fernandez, E. Miguel Gascón, M. Remmy, J. Richards, R. Scopigno, L. Vila, L. Wolf, H. Wright, M. Zallocco, K. Green, Developing the ArchAIDE application: a digital workflow for identifying, organising and sharing archaeological pottery using automated image recognition. *Internet Archaeol.* **52**, 1–48 (2020)
3. A. Aprile, G. Castellano, G. Eramo, Classification of mineral inclusions in ancient ceramics: comparing different modal analysis strategies. *Archaeol. Anthropol. Sci.* **11**(6), 2557–2567 (2019). <https://doi.org/10.1007/s12520-018-0690-y>
4. A. Aprile, G. Castellano, G. Eramo, Combining image analysis and modular neural networks for classification of mineral inclusions and pores in archaeological potsherds. *J. Archaeol. Sci.* **50**, 262–272 (2014). <https://doi.org/10.1016/j.jas.2014.07.017>
5. V. Barbin, K. Ramseyer, D. Decrouez, S.J. Burns, J. Chamay, J.L. Maier, Cathodoluminescence of white marbles: an overview. *Archaeometry* **34**(2), 175–183 (1992). <https://doi.org/10.1111/j.1475-4754.1992.tb00490.x>
6. P. Blanc, M.P. Lapuente Mercadal, A. Gutiérrez García-Moreno, A new database of the quantitative cathodoluminescence of the main quarry marbles used in antiquity. *Minerals* **10**(4), 381 (2020). <https://doi.org/10.3390/min10040381>
7. T. Blaschke, Object based image analysis for remote sensing. *ISPRS J. Photogramm. Remote Sens.* **65**(1), 2–16 (2010). <https://doi.org/10.1016/j.isprsjprs.2009.06.004>
8. S. Boggs, D. Krinsley, *Application of Cathodoluminescence Imaging to the Study of Sedimentary Rocks* (Cambridge University Press, 2006)
9. S. Boggs Jr., Y.I. Kwon, G.G. Goles, B.G. Rusk, D. Krinsley, A. Seyedolali, Is quartz cathodoluminescence color a reliable provenance tool? A quantitative examination. *J. Sediment. Res.* **72**(3), 408–415 (2002). <https://doi.org/10.1306/102501720408>

10. B. Carrión-Ruiz, S. Blanco-Pons, J.L. Lerma García, in *Digital image analysis of the visible region through simulation of rock art paintings. 8th International Congress on Archaeology, Computer Graphics, Cultural Heritage and Innovation*, pp. 169–175. Editorial Universitat Politècnica de València. <https://doi.org/10.4995/arqueologica8.2016.3560> (2016)
11. S. Cazenave, R. Chapoulie, G. Villeneuve, Cathodoluminescence of synthetic and natural calcite: the effects of manganese and iron on orange emission. *Mineral. Petrol.* **78**(3), 243–253 (2003). <https://doi.org/10.1007/s00710-002-0227-y>
12. R. Chapoulie, C. Déléry, F. Daniel, M. Venrell-Saz, Cuerda seca ceramics from al-andalus, islamic spain and portugal (10th– 12th centuries ad): investigation with sem–edx and cathodoluminescence. *Archaeometry* **47**(3), 519–534 (2005). <https://doi.org/10.1111/j.1475-4754.2005.00217.x>
13. R. Chapoulie, B. Robert, S. Casenave, The cathodoluminescence phenomenon used for the study of ancient ceramics and stones. *Cities Mem. Int. J. Cult. Herit. Risk* **1**(1), 53–72 (2016)
14. G. Dal Sasso, L. Maritan, S. Salvatori, C. Mazzoli, G. Artioli, Discriminating pottery production by image analysis: a case study of Mesolithic and Neolithic pottery from Al Khiday (Khartoum, Sudan). *J. Archaeol. Sci.* **46**, 125–143 (2014). <https://doi.org/10.1016/j.jas.2014.03.004>
15. M. Doneus, W. Neubauer, in 3D laser scanners on archaeological excavations. *Proceedings of the XXth international symposium CIPA*, Torino, pp. 226–231 (2005)
16. M. Emami, R. Chapoulie, K. Abdi, Cathodoluminescence microscopy for interpreting the fabric and heating process of ancient pottery: Preliminary study on the technological features of pottery from the Kur River basin. *Archaeometry* (2021). <https://doi.org/10.1111/arc.12718>
17. J. Goetze, D. Habermann, U. Kempe, R.D. Neuser, D.K. Richter, Cathodoluminescence microscopy and spectroscopy of plagioclases from lunar soil. *Am. Miner.* **84**(7–8), 1027–1032 (1999). <https://doi.org/10.2138/am-1999-7-804>
18. J. Götzte, M. Plötze, D. Habermann, Origin, spectral characteristics and practical applications of the cathodoluminescence (CL) of quartz—a review. *Mineral. Petrol.* **71**(3–4), 225–250 (2001). <https://doi.org/10.1007/s007100170040>
19. J. Götzte, H.P. Schertl, R.D. Neuser, U. Kempe, J.M. Hanchar, Optical microscope-cathodoluminescence (OM–CL) imaging as a powerful tool to reveal internal textures of minerals. *Mineral. Petrol.* **107**(3), 373–392 (2013). <https://doi.org/10.1007/s00710-012-0256-0>
20. M.L. Gualandi, R. Scopigno, L. Wolf, J. Richards, M. Heinzlmann, M.A. Hervas, J. Buxeda i Garrigos, L. Vila, M. Zallocco, in *ArchAIDE-archaeological automatic interpretation and documentation of cERamics. EUROGRAPHICS Workshop on Graphics and Cultural Heritage*, pp. 1–4. The Eurographics Association (2016)
21. A.M. Hunt, Development of quartz cathodoluminescence for the geological grouping of archaeological ceramics: firing effects and data analysis. *J. Archaeol. Sci.* **40**(7), 2902–2912 (2013). <https://doi.org/10.1016/j.jas.2013.02.030>
22. V.A. Knyaz, A.V. Gabouchian, Photogrammetry-based automated measurements for tooth shape and occlusion analysis. *Int. Arch. Photogram. Remote Sens. Spatial Inf. Sci.* **41**, 849 (2016)
23. K. Lambers, Airborne and spaceborne remote sensing and digital image analysis in archaeology. *Digit. Geoarchaeol.* (2018). [https://doi.org/10.1007/978-3-319-25316-9\\_7](https://doi.org/10.1007/978-3-319-25316-9_7)
24. H.W. Leverenz, *An Introduction to Luminescence of Solids* (Wiley, NY, 1950)
25. P.C. Livingood, A.S. Cordell, Point/counter point: the accuracy and feasibility of digital image techniques in the analysis of ceramic thin sections. *J. Archaeol. Sci.* **36**(3), 867–872 (2009). <https://doi.org/10.1016/j.jas.2008.11.015>
26. A. S. Marfunin, & N. G. Egorova, *Physics of minerals and inorganic materials: an introduction* (Berlin: Springer, 1979), pp. 209–213
27. L. Maritan, R. Piovesan, G. Dal Sasso, S. Baklouti, L. Casas, C. Mazzoli, L. Salmaso, L. Corain, Comparison between different image acquisition methods for grain-size analysis and quantification of ceramic inclusions by digital image processing: how much similar are the results? *Archaeol. Anthropol. Sci.* **12**(8), 1–15 (2020). <https://doi.org/10.1007/s12520-020-01096-0>
28. C. Oleari (ed.), *Misurare il Colore: Fisiologia Della Visione a Colori Fotometria Colorimetria e Norme Internazionali* (Hoepli, Italy, 2008)
29. E. Palamara, P.P. Das, S. Nicolopoulos, L.T. Cifuentes, A. Oikonomou, E. Kouloumpi, A. Terlix, N. Zacharias, Applying SEM-Cathodoluminescence imaging and spectroscopy as an advanced research tool for the characterization of archaeological material. *Microchem. J.* **158**, 105230 (2020). <https://doi.org/10.1016/j.microc.2020.105230>
30. P. Picouet, M. Maggetti, D. Piponnier, M. Schvoerer, Cathodoluminescence spectroscopy of quartz grains as a tool for ceramic provenance. *J. Archaeol. Sci.* **26**(8), 943–949 (1999). <https://doi.org/10.1006/jasc.1999.0421>
31. D. Piponnier, F. Bechtel, D. Florin, J. Molera, M. Schvoerer, M. Vendrell, Apport de la cathodoluminescence à l'étude des transformations de phases cristallines dans des céramiques kaoliniques carbonatées. *Key Eng. Mater.* **132–136**, 1470–1473 (1997)
32. G. Poggi, M. Buono, in *Enhancing Archaeological Interpretation with Volume Calculations. An Integrated Method of 3D Recording and Modeling. CAA2016: Oceans of Data: Proceedings of the 44th Conference on Computer Applications and Quantitative Methods in Archaeology*, p. 457. Archaeopress Publishing Ltd.
33. P.S. Quinn, *Ceramic Petrography: The Interpretation of Archaeological Pottery & Related Artefacts in Thin Section* (Archaeopress Publishing Ltd., Oxford, 2013)
34. W.S. Rasband, ImageJ, U. S. National Institutes of Health, Bethesda, Maryland, USA. <https://imagej.nih.gov/ij/>, 1997–2018
35. G. Remond, F. Cesbron, R. Chapoulie, D. Ohnenstetter, C. Roques-Carnes, M. Schvoerer, Cathodoluminescence applied to the microcharacterization of mineral materials: a present status in experimentation and interpretation. *Scanning Microsc.* **6**(1), 2 (1992)
36. T. Smith, J. Guild, The CIE colorimetric standards and their use. *Trans. Opt. Soc.* **33**(3), 73 (1931)
37. F. Stanco, S. Battiato, G. Gallo, *Digital Imaging for Cultural Heritage Preservation. Analysis, Restoration, and Reconstruction of Ancient Artworks* (CRC Press, USA, 2011)
38. M. Toffolo, G. Ricci, R. Chapoulie, L. Caneve, I. Kaplan-Ashiri, Cathodoluminescence and laser-induced fluorescence of calcium carbonate: a review of screening methods for radiocarbon dating of ancient lime mortars. *Radiocarbon* **62**(3), 545–564 (2020). <https://doi.org/10.1017/RDC.2020.21>
39. C. Weiß, M. Köster, S. Japp, Preliminary characterization of pottery by cathodoluminescence and SEM–EDX analyses: an example from the Yeha region (Ethiopia). *Archaeometry* **58**(2), 239–254 (2016). <https://doi.org/10.1111/arc.12165>
40. I.K. Whitbread, A. Hunt, Fabric Description of Archaeological Ceramics, in *The Oxford Handbook of Archaeological Ceramic Analysis*, ed. by A. Hunt (Oxford University Press, Oxford, 2017), pp. 200–216